

Finite size scaling of the Kuramoto model at criticality

Su-Chan Park (박수찬)*

Department of Physics, The Catholic University of Korea, Bucheon 14662, Republic of Korea

Hyunggyu Park (박형규)†

Quantum Universe Center, Korea Institute for Advanced Study, Seoul 02495, Republic of Korea

(Dated: June 28, 2024)

The asymptotic scaling behavior of the Kuramoto model with finite populations has been notably elusive, despite comprehensive investigations employing both analytical and numerical methods. In this study, we explore the Kuramoto model with “deterministic” sampling of natural frequencies, employing extensive numerical simulations and report the asymptotic values of the finite-size scaling (FSS) exponents, which deviate significantly from the previously reported values in the literature. Additionally, we observe that these exponents are sensitive to the specifics of the sampling method. We discuss the origins of this variability through the self-consistent theory of the entrained oscillators.

I. INTRODUCTION

The Kuramoto model [1], a prototypical model of synchronization, is a system of N interacting phase oscillators that evolve in a deterministic manner by the equation

$$\frac{d\theta_k}{dt} = \omega_k + \frac{K}{N} \sum_{j \in I} \sin(\theta_j - \theta_k), \quad (1)$$

where I is an index set with N elements, k is any element of I , θ_k is the phase of an oscillator indexed by k with a corresponding (time-independent) natural frequency ω_k , and K is the interaction parameter that is assumed to be positive (for a review, see, e.g, Ref. [2]). The natural frequencies under the infinite- N limit are assumed to satisfy

$$\lim_{N \rightarrow \infty} \frac{1}{N} \sum_{k \in I} \Theta(\omega_k - a) \Theta(b - \omega_k) = \int_a^b g(\omega) d\omega, \quad (2)$$

for any real numbers a and b with $a \leq b$, where $\Theta(x)$ is the Heaviside step function and $g(\omega)$ is a (normalized) frequency density function that also stipulates the Kuramoto model. In this paper, we limit ourselves to the mostly studied case that $g(\omega)$ is a continuous, symmetric, and unimodal function whose shape near $\omega \approx 0$ is concave and parabolic.

It is customary to introduce the phase order parameters

$$\Delta_N(t) := \frac{1}{N} \sum_{j \in I} e^{i\theta_j(t)}, \quad r_N(t) := |\Delta_N(t)|, \quad (3)$$

and to rewrite Eq. (1) as

$$\frac{d\theta_k}{dt} = \omega_k - K r_N(t) \sin(\theta_k - \psi(t)), \quad (4)$$

where the average phase angle, $\psi(t)$, is obtained from $\Delta_N(t) \equiv r_N(t) e^{i\psi(t)}$. The long-time behavior of the order parameters are defined as

$$R_N := \lim_{t \rightarrow \infty} \overline{r_N}(t), \quad R := \lim_{N \rightarrow \infty} R_N, \quad (5)$$

where $\overline{X}(t)$ denotes the time average of X , defined as $\overline{X}(t) := \frac{1}{t} \int_0^t X(t') dt'$. It is well known [1] that there exists a synchronization transition such that $R = 0$ for $K \leq K_c = 2/[\pi g(0)]$ and $R \sim (K - K_c)^\beta$ for $K > K_c$ with the order parameter exponent $\beta = \frac{1}{2}$.

The dynamic fluctuations of the order parameter can be defined as

$$\chi_N := N \lim_{t \rightarrow \infty} \left[\overline{r_N^2}(t) - \overline{r_N}(t)^2 \right], \quad \chi := \lim_{N \rightarrow \infty} \chi_N, \quad (6)$$

which are expected to behave as $\chi \sim |K - K_c|^{-\gamma}$ near the transition ($0 < |K - K_c| \ll 1$) with the fluctuation exponent γ .

For sufficiently small $\epsilon := |K - K_c|$ and for sufficiently large N , the leading behavior of R_N is expected as

$$R_N \sim \begin{cases} \epsilon^\beta \rho_+ (\epsilon^{\bar{\nu}_+} N), & \epsilon > 0, \\ |\epsilon|^\beta \rho_- (|\epsilon|^{\bar{\nu}_-} N), & \epsilon < 0, \\ N^{-\beta/\bar{\nu}_c}, & \epsilon = 0, \end{cases} \quad (7)$$

where ρ_\pm should satisfy

$$\lim_{x \rightarrow \infty} \rho_+(x) = \text{const}, \quad \lim_{x \rightarrow \infty} \rho_-(x) = 0,$$

to conform to the critical behavior of R . In what follows, we will refer to $\bar{\nu}_+$, $\bar{\nu}_-$, and $\bar{\nu}_c$ as the finite-size scaling (FSS) exponents for the supercritical region, for the subcritical region, and at the critical point, respectively. Needless to say, the infinite x limit above should be understood as the infinite N limit for fixed small ϵ .

If the conventional theory of critical phenomena is applicable to the Kuramoto model, one can claim $\bar{\nu}_+ =$

* spark0@catholic.ac.kr

† hgpark@kias.re.kr

$\bar{\nu}_- = \bar{\nu}_c$. Accordingly, there is no need to distinguish $\bar{\nu}$'s in Eq. (7) and the three exponents are usually denoted by a single exponent $\bar{\nu}$. In this case, it is a common numerical practice to estimate $\bar{\nu}$ by studying R_N only at the critical point. As we will see from Sec. V on, however, the three FSS exponents of the Kuramoto model may have different values at the corresponding regimes, depending on the sampling rule of natural frequencies. On this account, we will stick to use the three exponents for the FSS of R_N . Only when we refer to the exponent in the literature, we will use $\bar{\nu}$. Further discussion about the FSS exponents can be found in Sec. VII B.

Again by the conventional theory, one may expect the hyperscaling relation

$$\gamma = \bar{\nu} - 2\beta, \quad (8)$$

which should be correct unless the leading finite-size term in r_N^2 and \bar{r}_N^2 exactly cancel each other in Eq. (6).

It is well known that finite-size effects are influenced by the sampling methods of natural frequencies (see also Ref. [3, 4] for the same phenomenon in the uniformly distributed g). In particular, the values of the exponents $\bar{\nu}$ and γ may also vary depending on the specific details of samplings. In the literature, two typical samplings called *random* and *regular* samplings have been under consideration. In the random-sampling case, ω_k 's are independent and identically distributed (iid) random variables in accordance with the density $g(\omega)$. In the regular-sampling case, ω_k is determined by

$$\int_{-\infty}^{\omega_k} g(\omega) d\omega = \frac{k - 1/2}{N}, \quad (9)$$

with integer $k = 1, 2, \dots, N$, comprising the index set I . In Ref. [5], it was claimed that $\bar{\nu} = 5/2$ and $\gamma = 1$ for the random-sampling case, and $\bar{\nu} \simeq 5/4$ and $\gamma \simeq 1/4$ for the regular-sampling case. For the random-sampling case, these exponent values are well established through some analytic derivations [6–9] reinforced by extensive numerical simulations [5, 9, 10]. However, for the regular-sampling case, the exponent values are estimated mostly through numerical simulations for rather small size and short simulation time [5]. In this paper, we perform extensive numerical simulations for much bigger size and much longer simulation time to estimate the accurate exponent values in the asymptotic (large N) regime for more general “deterministic” sampling including the regular case. The main focus in this work will be on the scaling behavior of R_N , or, equivalently, on the value of $\bar{\nu}$ (more precisely, $\bar{\nu}$'s).

The structure of the paper is as follows. In Sec. II, we specify the form of $g(\omega)$ as well as the sampling method. In Sec. III, we explain details of the method in numerical analysis. In Sec. IV, we present our numerical results for the regular-sampling case, which will be called equally spaced case later. In particular, we will claim that our estimate of $\bar{\nu}_c$ is actually different from $\bar{\nu}$ in Ref. [5]. To grasp some analytic understanding, we study the self-consistent mean field equation in Sec. V. In Sec. VI, we

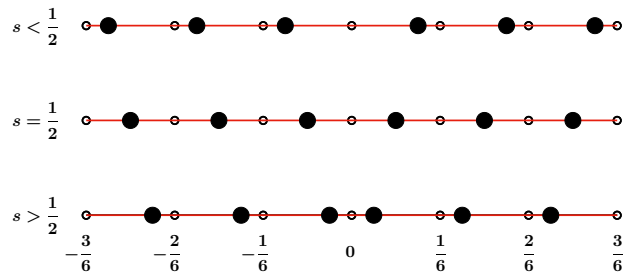


FIG. 1. Example of x_k 's with $N = 6$ for $s = \frac{1}{4} < \frac{1}{2}$, $s = \frac{1}{2}$, and $s = \frac{3}{4} > \frac{1}{2}$ (top to bottom). Filled circles indicate x_k 's of the corresponding s .

present numerical results for other sampling cases. In particular, we will claim another value of $\bar{\nu}_c$ that, as far as we are aware of, has never been reported in the literature. These various critical exponents are discussed in more detail in Sec. VII. We summarize and conclude the work in Sec. VIII.

II. FREQUENCY SAMPLINGS

In case $g(\omega)$ has an unbounded support, a certain oscillator can assume a very high frequency particularly when N is large. For example, if $g(\omega) = \pi^{-1}/(\omega^2 + 1)$ and $N = 2^{18}$ (the largest system size we used in our numerical studies), the largest frequency in the regular sampling is $\cot(\pi/2^{19}) > 10^5$, which is hard to be controlled in numerical integrations. Although no serious problem due to this difficulty has been reported, we would like to avoid any unexpected numerical uncertainty by too fast oscillations.

As the critical scaling only depends on the shape of $g(\omega)$ near $\omega \approx 0$ and overall unimodality, it would be numerically practical to consider a frequency density with a compact support. Specifically, we consider

$$g(\omega) = \frac{3}{2} (1 - 4\omega^2) \Theta(1 - 2|\omega|), \quad (10)$$

which gives $K_c = 4/(3\pi) \approx 0.4244$.

A set of N natural frequencies $\{\omega_k\}$ is sampled deterministically in the following way. For even $N = 2M$, it is convenient to take the index set as $I = \{\pm 1, \pm 2, \dots, \pm M\}$. To assign the frequency value ω_k for each index k , we first introduce

$$x_k = \begin{cases} (k - s)/N, & k > 0, \\ -x_{|k|}, & k < 0, \end{cases} \quad (11)$$

with a constant s in the range $0 \leq s \leq 1$ (see Fig.1). The ω_k is then determined through the relation

$$G(\omega_k) = x_k \quad (12)$$

with the function G defined by

$$G(\omega) := \int_0^\omega g(\omega') d\omega', \quad \text{for } \omega \geq 0. \quad (13)$$

As $g(-\omega) = g(\omega)$, G is naturally extended to all real numbers by $G(-\omega) = -G(\omega)$. Note that Eq. (12) can be inverted analytically with $g(\omega)$ given by Eq. (10), resulting in

$$\omega_k = G^{-1}(x_k) = \sin\left(\frac{1}{3} \sin^{-1}(2x_k)\right).$$

Through this type of sampling, we maintain the natural frequency symmetry even for finite N ; $\omega_{-k} = -\omega_k$. The $s = \frac{1}{2}$ case corresponds to the regular-sampling case in Eq. (9). We will refer to this case as the equally spaced (ES) case (equal interval between any two x_k 's in a row). Deviations from $s = \frac{1}{2}$ govern the non-uniformity of frequency distribution at the finite-size level near $\omega \approx 0$ (either thinning for $s < \frac{1}{2}$ or thickening for $s > \frac{1}{2}$, see Fig.1).

For odd $N = 2M + 1$, we take $I = \{0, \pm 1, \pm 2, \dots, \pm M\}$ with $x_0 = 0$, $x_k = (k - s + \frac{1}{2})/N$ for $k > 0$, and $x_{-k} = -x_k$. The $s = \frac{1}{2}$ case also corresponds to the ES case. The following conclusion for even N does not change for odd N as long as this rule with the same s is employed.

III. NUMERICAL METHODS

Exploring the FSS behavior near the criticality, especially for deterministic sampling of natural frequencies, is exceedingly challenging, due to huge computational costs. In previous studies for the regular sampling, simulations are limited up to a system size of $N = 25\,600$ and a simulation time of $t_{\max} \sim 10^5$ [5].

In our research, we extend these limits considerably to a much larger scale ($N = 262\,144$ and $t_{\max} \sim 10^9$) to reach the asymptotic scaling regime. Moreover, we enhance the reliability of our estimates for the FSS exponent values by employing an ‘‘effective-exponent’’ analysis of extensive numerical data, which incorporates corrections to scaling.

For convenience, the system size N is assumed even with $N = 2M$. Since $\omega_{-k} = -\omega_k$, it is convenient to rewrite the evolution equations with new variables $\phi_k := \frac{1}{2}(\theta_k - \theta_{-k})$ and $\sigma_k := \frac{1}{2}(\theta_k + \theta_{-k})$ as

$$\begin{aligned} \frac{d\phi_k}{dt} &= \omega_k - Kr_N \cos(\sigma_k - \psi) \sin(\phi_k), \\ \frac{d\sigma_k}{dt} &= -Kr_N \sin(\sigma_k - \psi) \cos(\phi_k), \end{aligned}$$

where $k = 1, 2, \dots, M$. From the above equation, one can easily deduce that if we adopt a ‘symmetric’ initial configuration with $\sigma_k(0) = \psi(0) = \psi_0$ (constant) for all k , then $\sigma_k(t) = \sigma_k(0)$ for all t . Without losing generality, we can set $\psi_0 = 0$ and we have the symmetry $\theta_{-k}(t) = -\theta_k(t)$ for all k and t .

As long as $\lim_{N \rightarrow \infty} \ln R_N / \ln N$ at criticality is well-defined (with the value $-\beta/\bar{\nu}_c$), we expect that an initial condition would not affect the value of $\bar{\nu}_c$. In this regard, we choose the symmetric initial configuration that gives $\theta_k = \phi_k = -\theta_{-k}$ and rewrite the equation with rescaled time $\tau := Kt$ as (k is positive)

$$\Delta_N = \frac{1}{M} \sum_{k=1}^M \cos \theta_k, \quad \frac{d\theta_k}{d\tau} = \nu_k - \Delta_N \sin \theta_k, \quad (14)$$

where we have used rescaled frequencies $\nu_k := \omega_k/K$. This equation obviously reduces computational efforts. With this symmetric initial condition, the order parameter Δ_N becomes always real and the average phase angle $\psi(t)$ assumes only 0 or π , corresponding to positive or negative $\Delta_N(\tau)$, respectively. We confirmed numerically that alternative initial conditions with broken symmetry (for example, random ϕ_k and σ_k at $t = 0$) also converge to the same values of the FSS exponents (not shown here).

For numerical integration of Eq. (14), we employ the 4th order Runge-Kutta method with time step size $d\tau = 0.05$. As the initial conditions, we set $\theta_k(0) = 0$ for all $k \in I$ in most cases. To ascertain the stationary-state values of the order parameters, we disregard the data from the transient regime up to $\tau = \tau_s$ and collect the data over the interval $\tau_s < \tau \leq \tau_s + \tau_{\max}$ with $\tau_{\max} = 5 \times 10^8$ (in terms of the original time, the maximum time is about $t_{\max} \approx 10^9$). We set $\tau_s = 10^3 N^{2/3}$ to ensure the system has reached a stationary state, which is supported both numerically and through theoretical analysis detailed in Sec. VI.

In the stationary state, we calculate the time average of $r_N(\tau)$ as

$$\tilde{R}_N(\tau) = \frac{1}{\tau} \sum_{i=1}^{\tau} r_N(i + \tau_s), \quad (15)$$

where $1 \leq \tau \leq \tau_{\max}$. Note that data sampling in average does not occur at every time step, but rather at every integer value of τ to reduce correlations between neighboring data points. Its statistical error is determined by the difference between the maximum and the minimum of the set $\{\tilde{R}_N(\tau) : 3 \times 10^8 \leq \tau \leq 5 \times 10^8\}$. To support numerical reliability, numerical integrations with a larger step size $d\tau = 0.1$ were also performed, to observe no significant differences in the time averaged quantities (not shown here).

We consider various system sizes, specifically $N = 2^5, 2^6, \dots, 2^{18}$ for $s = 0, \frac{1}{4}, \frac{1}{2}, \frac{3}{4}$, and 1. Our primary focus is on the critical FSS at $K = K_c = 4/(3\pi)$, where an averaged quantity R_N scales for large N as

$$R_N = aN^{-\beta/\bar{\nu}_c} [1 + BN^{-c_R} + o(N^{-c_R})], \quad (16)$$

with the leading correction-to-scaling (CTS) exponent c_R , where a, B are constants and $o(f(N))$ denotes higher-order terms beyond $f(N)$.

With a sequence of R_N values for various N , we determine $-\beta/\bar{\nu}_c$ as well as c_R in the following manner. For a positive $b > 1$, the effective exponent ξ^{eff} is defined as

$$\xi^{\text{eff}}(N; b) := \frac{\ln R_N - \ln R_{N/b}}{\ln b}, \quad (17)$$

which behaves for large N as

$$\xi^{\text{eff}}(N; b) = -\frac{\beta}{\bar{\nu}_c} - B \frac{b^{c_R} - 1}{\ln b} N^{-c_R} + o(N^{-c_R}). \quad (18)$$

Plotting ξ^{eff} as a function of N^{-c_R} results in a straight line for large N , enabling the estimation of $-\beta/\bar{\nu}_c$ via simple linear extrapolation. Therefore, accurate information regarding to the CTS exponent c_R is essential for obtaining a precise estimate of $-\beta/\bar{\nu}_c$.

To determine c_R independently, we employ the method introduced by one of the authors [11, 12]. We define the CTS function Q_R as

$$Q_R(N; b) := \left| \log R_N + \ln R_{N/b^2} - 2 \ln R_{N/b} \right| \quad (19) \\ = (b^{c_R} - 1)^2 |B| N^{-c_R} + o(N^{-c_R}),$$

which indicates that the plots of $Q_R(N; b)/(b^{c_R} - 1)^2$ against N should converge onto a single curve, independent of b , for large N , if the correct value of c_R is used. By adjusting c_R to achieve this convergence in the asymptotic regime for various values of b , we can estimate c_R without information about $-\beta/\bar{\nu}_c$. This estimate can be further validated by measuring the slope in the log-log plot, as illustrated in the inset of Fig. 2. With this value of c_R , we can accurately estimate the FSS exponent $\bar{\nu}_c$, using Eq. (18).

IV. NUMERICAL ESTIMATE OF $\bar{\nu}_c$ FOR THE ES ($s = \frac{1}{2}$) CASE

In previous numerical studies [5, 13], the FSS exponents for the ES case (regular sampling) were suggested to be $-\beta/\bar{\nu} \approx -2/5$ and $\gamma/\bar{\nu} \approx 1/5$. A notable feature of these estimates is their adherence to the hyperscaling relation in Eq. (8). Additionally, $\gamma = 1/4$ was analytically predicted in [13] as $K - K_c \rightarrow 0^+$. However, the numerical estimates were obtained from relatively small-scale data both in terms of system size and simulation time ($N = 25\,600$ and $t_{\text{max}} \sim 10^5$) [5], thus not fully convincing. In our study, the maximum system size ($N = 2^{18}$) is approximately 10 times larger than that in the previous study [5]. To ensure the larger system to reach a stationary state and to collect sufficient stationary-state data, we perform significantly longer simulations, extending up to $t_{\text{max}} \approx 10^9$, which is approximately 10^4 times longer.

Our numerical results are presented in Fig. 2, where the effective exponents $\xi^{\text{eff}} = -(\beta/\bar{\nu}_c)_{\text{eff}}$ are plotted against N^{-c_R} , with the estimated CTS exponent $c_R = 0.3$. In the inset, we display $Q_R/(b^{0.3} - 1)^2$ plotted against N for $b = 4, 8, \text{ and } 16$ on a double-logarithmic scale, which

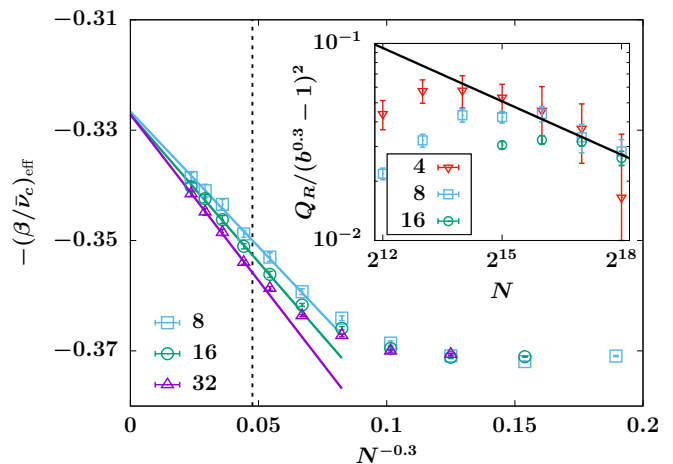


FIG. 2. Plots of $-(\beta/\bar{\nu}_c)_{\text{eff}}$ vs $N^{-0.3}$ for $s = \frac{1}{2}$ with $b = 8$ (square), 16 (circle), and 32 (triangle). The straight lines on each dataset depict the results of the linear fitting. The dashed vertical line indicates the position of the largest size ($N = 25\,600$) studied in Ref. [5]. Inset: Double-logarithmic plots of $Q_R/(b^{0.3} - 1)^2$ vs N for $b = 4$ (reverse triangle), 8 (square), 16 (circle). The straight line with slope -0.3 is for a guide to the eyes.

demonstrates a tendency for the data collapse onto a straight line with slope -0.3 in the asymptotic regime of $N \gtrsim 2^{16}$. This behavior supports the choice of $c_R \approx 0.3$, independently of $\beta/\bar{\nu}_c$.

For large N , Eq. (18) predicts that the effective exponent $(\beta/\bar{\nu}_c)_{\text{eff}}$ approaches the asymptotic value $\beta/\bar{\nu}_c$ linearly in terms of N^{-c_R} with b -dependent slopes. These predictions are consistent with numerical data shown in Fig. 2. Linear fitting for $N \geq 2^{15}$ yields a consistent value of

$$\beta/\bar{\nu}_c = 0.325(15) \approx \frac{1}{3}, \quad \text{thus } \bar{\nu}_c = 1.54(7) \approx \frac{3}{2}, \quad (20)$$

irrespective of the choice of b . These values are clearly distinct from $2/5$ and $5/4$, suggested in [5].

Notably, $(\beta/\bar{\nu}_c)_{\text{eff}}$ for small N remains nearly constant around 0.37, which is comparable to the estimate $\beta/\bar{\nu} = 0.39(2)$ from Ref. [5]. However, it is evident that $(\beta/\bar{\nu}_c)_{\text{eff}}$ eventually drifts toward a smaller value approximately 0.325, as N increases. This late crossover to the asymptotic scaling regime renders the estimation of the FSS exponent exceedingly challenging. It also accounts for the delayed onset of the power-law scaling of Q_R , as observed in the inset of Fig. 2.

V. SOLUTIONS OF THE SELF-CONSISTENT EQUATION FOR ENTRAINED OSCILLATORS

To pursue analytic understanding of the numerical results in the previous section, this section investigates the mean-field self-consistent equation (MFSCE) for an arbitrary value of s . As usual, we assume that the order

parameter $\Delta_N(t)$ approaches a constant value $R_N e^{i\psi_0}$ in the long-time limit (mean field assumption). Then, the dynamic equations of Eq. (4) become completely decoupled with unknown R_N and their solutions are categorized into two distinct types. Oscillators with $|\omega_k| < KR_N$ eventually stabilize at fixed angles θ_k^e (entrained oscillators), satisfying $\omega_k = KR_N \sin \theta_k^e$ (we set $\psi_0 = 0$ without loss of generality). In contrast, oscillators with $|\omega_k| > KR_N$ continue to oscillate with modified frequencies (running oscillators).

By substituting these solutions into Eq. (3) and neglecting the contribution from running oscillators, we arrive at the MFSCE

$$R_N = \frac{1}{N} \sum_{k \in I^e} \sqrt{1 - \frac{\omega_k^2}{K^2 R_N^2}}, \quad (21)$$

where I^e denotes the index set of entrained oscillators ($|\omega_k| < KR_N$). In this formulation, the contribution of running oscillators are disregarded to avoid seemingly intractable complexity. Given that the contribution of running oscillators is at least $O(1/\sqrt{N})$ (representing independent random oscillators), any solutions of the MFSCE at lower orders are meaningless. Thus, we seek solutions only for $R_N \gg 1/N$ in the perturbation expansion.

For convenience, we define the following functions

$$S(z) := \frac{1}{N} \sum_{k \in I} \Theta(z^2 - \omega_k^2) \sqrt{1 - \frac{\omega_k^2}{z^2}}, \quad (22)$$

$$J(z) := \int_{-z}^z g(\omega) \sqrt{1 - \frac{\omega^2}{z^2}} d\omega, \quad (23)$$

where $z > 0$. It is clear that $J(z) = \lim_{N \rightarrow \infty} S(z)$. With $g(\omega)$ as given in Eq. (10), we obtain explicitly $J(z) = \frac{3}{4}\pi z(1 - z^2)$.

Introducing the abbreviation $Z := KR_N$, we rewrite the MFSCE, Eq.(21), as

$$\frac{Z}{K} = \frac{1}{N} \sum_k \Theta(Z^2 - \omega_k^2) \sqrt{1 - \frac{\omega_k^2}{Z^2}} = S(Z), \quad (24)$$

which becomes, in the $N \rightarrow \infty$ limit,

$$\frac{Z}{K} = \frac{3}{4}\pi Z(1 - Z^2). \quad (25)$$

The solution of Eq. (25) is

$$K_c = \frac{4}{3\pi}, \quad R = \begin{cases} K^{-3/2} \sqrt{K - K_c}, & K \geq K_c, \\ 0, & K < K_c, \end{cases} \quad (26)$$

which is consistent with $K_c = 2/[\pi g(0)]$ and $\beta = \frac{1}{2}$.

We now examine the finite-size corrections, specifically how much $S(Z)$ deviates from $J(Z)$ for large N . After a rather lengthy algebra (details are provided in Appendix A), we find

$$S(Z) \approx J(Z) + \frac{2s-1}{N} + \frac{\eta_0(\alpha)}{\sqrt{g(0)ZN^3}}, \quad (27)$$

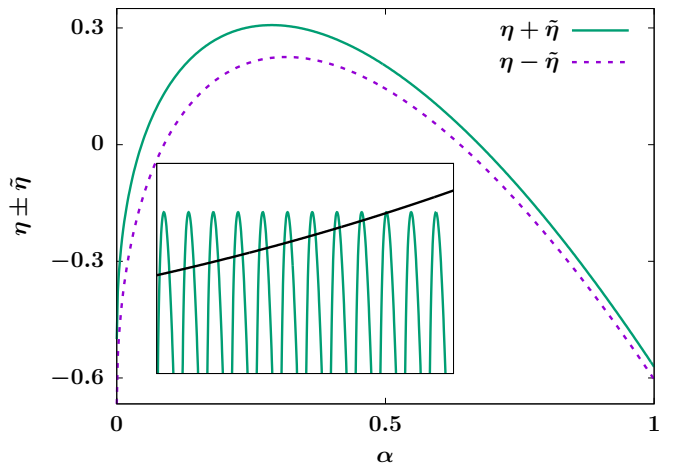


FIG. 3. Plots of $\eta + \tilde{\eta}$ (top) and $\eta - \tilde{\eta}$ (bottom) vs α . Since $-\tilde{\eta}(\alpha) \leq \eta_1(\alpha) \leq \tilde{\eta}(\alpha)$, there should be a region where $\eta_0(\alpha)$ is positive. Inset: Schematic graph to find solutions of Eq. (29). The continuous curve depicts $y = x^{7/2}$.

where the $O(1)$ parameter α is defined as

$$\alpha := N [G(Z) - x_{k_m}], \quad k_m := \max\{k : \omega_k \leq Z\},$$

which represents the N -scaled distance in the x_k space between the integral upper bound Z and the largest natural frequency of the entrained oscillators ω_{k_m} . The coefficient η_0 is given as $\eta_0 = \eta + \eta_1$ with

$$\eta(\alpha) = \sqrt{8\alpha} - \frac{2(1+2\alpha)^{3/2}}{3} + \frac{1}{12\sqrt{1+2\alpha}}$$

$$|\eta_1(\alpha)| \leq \tilde{\eta}(\alpha), \quad \tilde{\eta}(\alpha) := \frac{1}{12}(1+2\alpha)^{-3/2}.$$

Note that we have only bounds for η_1 , which is actually enough for our purpose.

Now the MFSCE becomes

$$\frac{Z}{K} \approx \frac{Z}{K_c}(1 - Z^2) + \frac{2s-1}{N} + \frac{\eta_0(\alpha)}{\sqrt{g(0)ZN^3}}. \quad (28)$$

Note that the first correction term always dominates over the second one for $Z \gg 1/N$ except for $s = \frac{1}{2}$.

In deriving Eq. (27), we have noticed three sets of oscillators for which the finite-size corrections exhibit different features; (1) most of oscillators with equally spaced x_k 's, (2) two oscillators in the edge region near $|\omega| \lesssim Z$, and (3) a few oscillators that break the equally spacing feature. The set (1) contributes leading behavior $J(z)$ as well as the second order correction. The second order correction also arises from the set (2). The first order correction is from the set (3); see also Sec. VII A for further discussion about the set (3) in other schemes.

A. ES case ($s = 1/2$)

We begin with analyzing the ES case ($s = \frac{1}{2}$) at the critical point $K = K_c$, which yields

$$Z^{7/2} \approx K_c \frac{\eta_0(\alpha)}{\sqrt{g(0)N^3}}. \quad (29)$$

Since α is also a function of Z , we have to resort to a graphical method to analyze Eq. (29). In Fig. 3, we plot $\eta(\alpha) \pm \tilde{\eta}(\alpha)$ versus α that provide bounds for η_0 . Since there is surely a region where η_0 is positive, Eq. (29) must have a solution.

Observe that α is a (pseudo-)periodic function of Z in that $\alpha(Z + \delta Z) = \alpha(Z)$ if $NG(Z + \delta Z) - NG(Z) = 1$. As $G(Z) \approx g(0)Z$ for small Z in Eq. (13), the period of $\alpha(Z)$ is approximately $1/[Ng(0)]$; see the inset of Fig. 3. There are multiple solutions of Eq. (29) (in fact, the number of solutions is $O(N^{4/7})$) and the largest one should be $O(N^{-3/7})$. Although the selection of solutions would depend on the initial condition in this framework, it may not be worthy to discuss ‘the’ solution under the presence of noisy running oscillators. Nonetheless, one may conclude that within the MFSCE the order parameter R_N should be bounded from above (largest solution), thus $\beta/\bar{\nu}_c \geq 3/7$ or $\bar{\nu}_c \leq 7/6 \approx 1.17$.

Note that this result is clearly inconsistent with our numerically obtained value of $\beta/\bar{\nu}_c \approx 0.33$ or $\bar{\nu}_c \approx 1.54$ in Sec. IV and also with the previous estimates of $\beta/\bar{\nu} = 0.4$ or $\bar{\nu} = 1.25$ in [5]. This implies that running oscillators cannot be neglected and their contributions to R_N may dominate the finite-size effects.

B. $s \neq 1/2$

For $s \neq \frac{1}{2}$, we rewrite the MFSCE, Eq. (27), as

$$R_N \approx \frac{K}{K_c} R_N (1 - K^2 R_N^2) + \frac{2s-1}{N}, \quad (30)$$

where the higher-order term is ignored for solutions with $R_N \gg 1/N$. For $K > K_c$, one can easily find

$$R_N \approx \sqrt{\frac{K-K_c}{K^3}} \left(1 + \frac{K_c K^{3/2}}{(K-K_c)^{3/2}} \frac{2s-1}{2N} \right), \quad (31)$$

up to the leading order in the finite-size corrections. In comparison to the scaling ansatz in Eq. (7), the MFSCE predicts $\bar{\nu}_+ = \frac{3}{2}$ for $s \neq \frac{1}{2}$. In Sec. VIA, we will argue, based on the simulation at criticality for $s > \frac{1}{2}$, that the MFSCE prediction is right for $s \neq \frac{1}{2}$ in the supercritical region. It is notable that numerically obtained $\bar{\nu}_c$ for the ES case is very close to the prediction of $\bar{\nu}_+$ by the MFSCE for $s \neq \frac{1}{2}$.

The qualitative behavior of R_N for $N \ll (K - K_c)^{-3/2}$ is quite different, depending on the sign of $s - \frac{1}{2}$. When $s > \frac{1}{2}$, the solution of R_N in Eq. (31) is well defined for

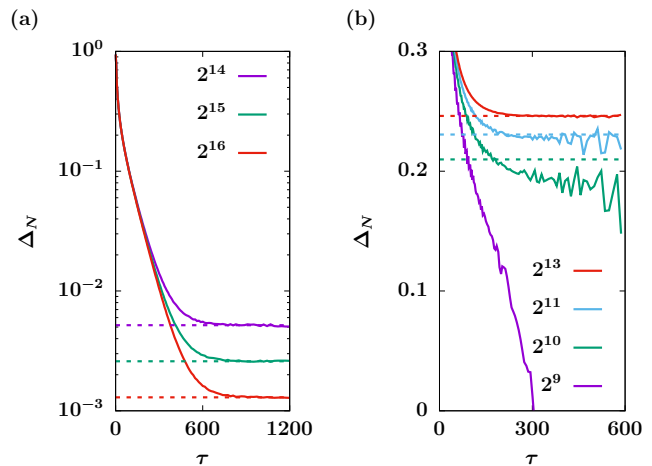


FIG. 4. (a) Semilogarithmic plots of Δ_N vs τ for $s = 1$ and $K = K_c - 0.005$ (subcritical). The system sizes are $N = 2^{14}$, 2^{15} , and 2^{16} (top to bottom). Dashed horizontal lines indicate the values of Eq. (33) for $N = 2^{14}$, 2^{15} , and 2^{16} (top to bottom), which show an excellent agreement with the saturating values of numerical integrations. (b) Plots of Δ_N vs τ for $s = 0$ and $K - K_c = 0.005$. The system sizes are $N = 2^9$, 2^{10} , 2^{11} , and 2^{13} (bottom to top). Dashed horizontal lines indicate the values of Eq. (31) for $N = 2^{10}$, 2^{11} , and 2^{13} (bottom to top). The predicted R_N for $N = 2^{13}$ shows an excellent agreement with the numerical data.

any N . In particular, Eq. (30) for $K = K_c$ has a solution as

$$R_N \approx \left(\frac{2s-1}{K_c^2} \right)^{1/3} N^{-1/3}, \quad (32)$$

which predicts $\beta/\bar{\nu}_c = \frac{1}{3}$, consistent with the conventional scaling theory $\bar{\nu}_+ = \bar{\nu}_c$. In this case, R_N is nonzero even in the subcritical region ($K \lesssim K_c$), where we get

$$R_N \approx \frac{K_c}{K_c - K} \frac{2s-1}{N}. \quad (33)$$

Note that the higher-order term $1/\sqrt{R_N N^3} \sim \sqrt{K_c - K}/N$ is negligible in comparison with $1/N$ in the regime ($|K - K_c| \ll 1$) we are interested in. In comparison to the scaling ansatz in Eq. (7), the MFSCE also predicts $\bar{\nu}_- = \frac{3}{2}$ for $s \neq \frac{1}{2}$. That is, the MFSCE for $s > \frac{1}{2}$ predicts a single FSS exponent just like the conventional theory.

In Fig. 4(a), we compare the numerical integration of Eq. (14) to the MFSCE prediction, Eq. (33), for $K = K_c - 0.005$ (subcritical) with $s = 1$. In contrary to the ES case, even Eq. (33) is in a perfect agreement with the numerical results without any correction from running oscillators up to the observed time in the figure. If Eq. (33) indeed prevails for all sufficiently large N and for all time, the MFSCE would predict correct $\bar{\nu}_-$ for $s > \frac{1}{2}$ and the conventional scaling theory (a single FSS exponent $\bar{\nu}$) would be applicable to this case.

Due to the condition $R_N \gtrsim N^{-1/2}$ to neglect running oscillators, however, $K_c - K$ must be necessarily smaller than $N^{-1/2}$ for Eq. (33) to be valid. Since the scaling ansatz should be applicable for all sufficiently large N with $|K - K_c|$ small and fixed, the running oscillators will eventually dominate as N gets larger and, in turn, the prediction (33) will eventually fail. If this scenario is right, the seemingly successful prediction of the MFSCE in Fig. 4(a) can be argued that the fluctuations by running oscillators are not fully developed up to the observed time.

Once the contribution by running oscillators becomes dominant, the subcritical scaling function cannot be given by Eq. (33), for the size of R_N is at least $O(1/\sqrt{N})$. In fact, performing longer simulation than in Fig. 4(a) revealed that the seeming stationary behavior becomes disrupted at late time and Δ_N goes way down to negative, implying the running oscillators become dominant. Accordingly, \bar{v}_- may be different from \bar{v}_+ . This is clearly an interesting question in that the critical scaling of the Kuramoto model may not be described by the conventional scaling theory. Since this question is beyond the scope of this work, we defer the full analysis of off-critical behavior to a later publication.

Let us move on to the case with $s < \frac{1}{2}$. At criticality and in the subcritical region ($K \leq K_c$), there is no proper solution for $R_N \gg 1/N$. Thus, running oscillators should be recalled to find any sensible value of R_N . In other words, the MFSCE for $s < \frac{1}{2}$ fails to predict \bar{v}_c and \bar{v}_- .

Even in the supercritical region ($K > K_c$), Eq. (31) does not make sense for $N(K - K_c)^{3/2} \ll 1$ because the resulting R_N becomes negative. Thus, Eq. (31) is meaningful only for sufficiently large N even in the supercritical region. In Fig. 4(b), we present numerically integrated results for $s = 0$ and $K = K_c + 0.005$ for various N 's. We observe that Δ_N for $N = 2^9$ crosses zero in short time even though $K > K_c$, implying an easy escape from the fixed point for positive Δ_N . For $N \geq 2^{10}$, Δ_N seems to saturate to a nonzero value, which does not match with the value from Eq. (31) for $N \leq 2^{11}$. Only for $N = 2^{13}$, the saturated value becomes consistent with the prediction from Eq. (31). Note that $N(K - K_c)^{3/2} \approx 2.90$ with $N = 2^{13}$.

VI. MORE NUMERICAL RESULTS

This section analyzes numerical data at criticality for various s , to find \bar{v}_c . We begin with presenting results for the case with $s > 1/2$ in which the MFSCE seems working quite well.

A. $s > 1/2$

We first present the early-time behavior Δ_N ($\tau \leq \tau_s$). Recall that $\theta_k(0) = 0$ for all k and, therefore, $\Delta_N(0) = 1$. At the critical point for the infinite number of oscillators,

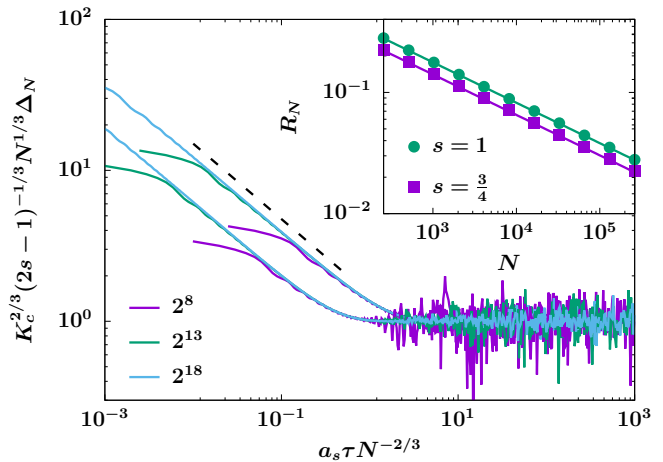


FIG. 5. Double logarithmic plots of $K_c^{2/3}(2s-1)^{-1/3}N^{1/3}\Delta_N$ vs $a_s\tau N^{-2/3}$ for $N = 2^8, 2^{13}, 2^{18}$ and for $s = 1$ (left three curves) and $s = \frac{3}{4}$ (right three curves). For clean visibility, we set the different value of a_s for different s as $a_s = 0.4$ for $s = 1$ and $a_s = 1$ for $s = \frac{3}{4}$. The dashed line with slope -0.5 is for guides to the eyes. Inset: Double logarithmic plots of R_N vs N for $s = 1$ (solid circle) and $s = \frac{3}{4}$ (solid square). Error bars are smaller than the symbol size. Corresponding straight lines depict $(2s-1)^{-1/3}K_c^{-2/3}N^{-1/3}$.

we expect

$$\frac{dR}{d\tau} \propto -R^3, \quad (34)$$

which predicts $R(\tau) \sim \tau^{-1/2}$. If Δ_N indeed approaches R_N in Eq. (32), there should be a typical time scale τ_c such that $\tau_c^{-1/2} \sim N^{-1/3}$ or $\tau_c \sim N^{\bar{z}}$ with the dynamic exponent $\bar{z} = \frac{2}{3}$. If this is the case, a plot of $K_c^{2/3}(2s-1)^{-1/3}\Delta_N(\tau)N^{1/3}$ against $\tau/N^{2/3}$ would exhibit a data collapse, where the prefactor in front of Δ_N is motivated from Eq. (32). To confirm this, we display the collapse plots in Fig. 5 for $s = \frac{3}{4}$ and $s = 1$, to observe perfect data collapses. For a better visibility, we multiply an arbitrary factor in front of τ in Fig. 5. It is remarkable that the saturating value in Fig. 5 is almost 1, consistent with the quantitative prediction in Eq. (32). This characteristic time scale is the motivation of choosing N dependent $\tau_s = 10^3 N^{2/3}$ in Sec. III.

In the stationary state, the data become very noisy, which signals development of large fluctuations by running oscillators. We study R_N by time averaging of $r_N(\tau)$ in the stationary state. In the inset of Fig. 5, we plot R_N against N for $s = \frac{3}{4}$ and $s = 1$. For comparison, we also draw the result from Eq. (32), which shows a nice coincidence. Since the prediction of Eq. (32) is so good, we do not show the analysis of the effective exponent and conclude $\bar{v}_c = \frac{3}{2}$ for $s > \frac{1}{2}$.

By our choice of the initial condition that gives $\theta_{-k}(t) = -\theta_k(t) \pmod{2\pi}$ for all t , the system now has at most Z_2 symmetry (invariant only under $\theta_k \mapsto \pi + \theta_k$) rather than the continuous $U(1)$ symmetry. Just like

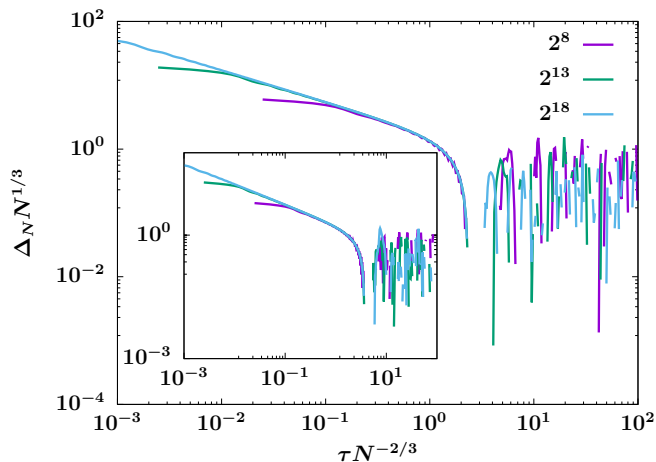


FIG. 6. Double-logarithmic plots of $N^{1/3} \Delta_N$ vs $\tau N^{-2/3}$ for $s = 0$ and for $N = 2^8, 2^{13},$ and 2^{18} . All curves around $\tau N^{-2/3} \sim 1$ collapse well into a single curve. The region without data points means Δ_N is negative. Inset: Similar plots with the same number of oscillators for $s = \frac{1}{4}$.

the Ising model equipped with dynamics (for instance, model A of Ref. [14]), it may still be possible for Δ_N to change its sign by fluctuations. Within our simulation time, however, we observed that $\Delta_N(\tau) = r_N(\tau)$ for all τ when $N \geq 2^{12}$. In other words, Δ_N did not change its sign up to $\tau = \tau_s + \tau_{\max}$ for large N . Even for smaller N , $\overline{\Delta_N}(\tau)$ is slightly different from $\overline{r_N}(\tau)$ (the size of difference is order of 10^{-6} for $N = 32$).

Being deterministic, it is not at all obvious whether this observation can be interpreted as a spontaneous Z_2 symmetry breaking or the dynamic equation never allows that all the entrained oscillators to change its phase by π . This question is clearly beyond the scope of our paper and we will not pursue it any further.

Since R_N in the supercritical region should be more stable than that at criticality, stability of the MFSCE solution at criticality (at least for long time) clearly suggests that in the supercritical region for $s \neq \frac{1}{2}$ with sufficiently large N , R_N will be well approximated by the MFSCE and $\bar{\nu}_+$ is indeed $\frac{3}{2}$ for any s different from $\frac{1}{2}$ (including small s). Our preliminary numerical investigation also supports this claim, which will be reported elsewhere.

B. $s < \frac{1}{2}$

We begin with the early time behavior. In Fig. 6, we plot $N^{1/3} \Delta_N$ against $\tau N^{-2/3}$ on a double logarithmic scale for $s = 0$ (main figure) and for $s = \frac{1}{4}$ (inset). Absence of data points in some region simply means Δ_N is negative there. All curves collapse perfectly into a single curve (for each s) before getting noisy. Although the MFSCE at the critical point does not give a proper solution for this case, $\bar{\nu}_+ = \frac{3}{2}$ still plays the role in determining

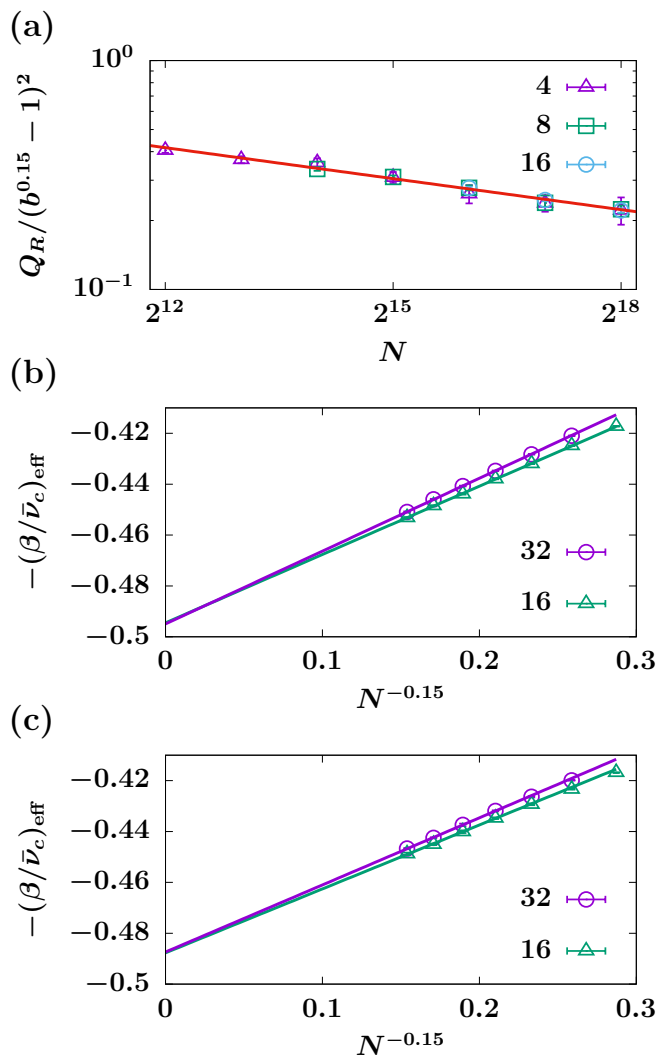


FIG. 7. (a) Double-logarithmic plots of $Q_R/(b^{0.15} - 1)^2$ vs N with $b = 4, 8, 16$ for $s = 0$. The straight line with slope -0.15 is for guides to the eyes. (b) Plots of $-(\beta/\bar{\nu}_c)_{\text{eff}}$ vs $N^{-0.15}$ for $s = 0$. (c) Plots of $-(\beta/\bar{\nu}_c)_{\text{eff}}$ vs $N^{-0.15}$ for $s = \frac{1}{4}$. In (b) and (c), the straight lines show the linear fitting results of the corresponding datasets.

the typical size and time scales of the system in the early time regime. The fact that Δ_N drops abruptly in an exponential way combined with the absence of a proper solution in the MFSCE at criticality suggests that there are, if exists, only a few entrained oscillators and running oscillators play a decisive role in the long time behavior of the order parameters. We will further discuss the implication of this observation in Sec. VII B.

In Fig. 7(a), we depict $Q_R/(b^{0.15} - 1)^2$ for $s = 0$ as a function of N for different values of b , to observe the same asymptotic behavior for large N regardless of b . We, therefore, conclude $c_R = 0.15$. The Q_R for $s = \frac{1}{4}$ shows a similar power-law behavior to Fig. 7(a) and we do not present details here. With the obtained c_R , we depict $-(\beta/\bar{\nu}_c)_{\text{eff}}$ as a function of N^{-c_R} for $s = 0$ [Fig. 7(b)]

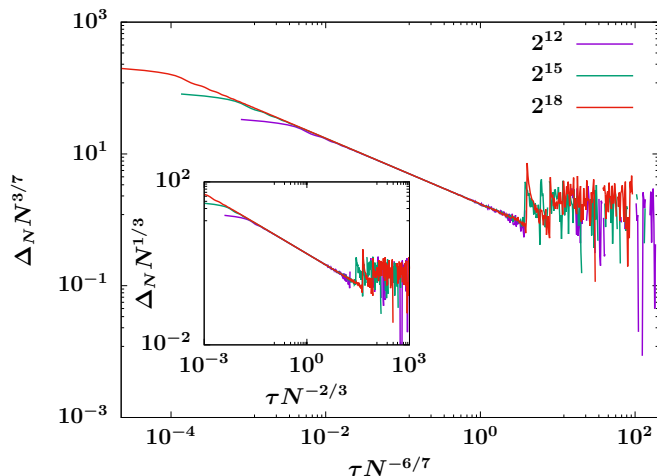


FIG. 8. Plots of $\Delta_N N^{3/7}$ vs $\tau N^{-6/7}$ for $s = \frac{1}{2}$ with $N = 2^{12}$, 2^{15} , and 2^{18} on a double logarithmic scale. Inset: Double-logarithmic plots of $\Delta_N N^{1/3}$ vs $\tau N^{-2/3}$ for the same data of the main figure.

and $s = \frac{1}{4}$ [Fig. 7(c)], respectively, for $b = 16$ and 32 . From the fitting, we conclude that $\beta/\bar{\nu}_c = 0.49(1)$ or $\bar{\nu}_c = 1.02(2)$ for both $s = 0$ and $\frac{1}{4}$, which is obviously different from the supercritical $\bar{\nu}_+$.

The value $\beta/\bar{\nu}_c \approx 0.5$ is reminiscent of the order parameter in case that all phases are iid random variables with uniform distribution in the interval $(0, 2\pi)$. If the randomness is indeed the reason of the value $0.49(1)$, we would expect $\gamma = 0$. Our preliminary simulations, not unexpectedly, suggest that γ is nonzero. Hence, the behavior of Δ_N cannot be interpreted as a fully random behavior of oscillators. Detailed analysis of fluctuations will be reported elsewhere.

C. Equally spaced case ($s = \frac{1}{2}$)

We have already seen that $\bar{\nu}_c$ is not explained by the MFSCE for the ES case. By the study in the previous subsection, however, it is still worth to ask whether the anticipated upper bound of $\bar{\nu}_c$ from the MFSCE can play any role in the early time region at criticality. Also it is natural to examine whether Δ_N saturates to a finite value (even though ‘the’ solution of the MFSCE cannot be fixed solely by the MFSCE) as in the case of $s > \frac{1}{2}$ or decays exponentially just like the case of $s < \frac{1}{2}$.

Since our simulation starts from $\Delta_N(0) = 1$, it seems plausible to expect that the system would saturate at the largest solution of the MFSCE and, therefore, $7/6$ of the MFSCE would play a role in the early time regime. Also by the same logic given in the beginning of Sec. VIA, we would have the dynamic exponent to be $\bar{z} = 6/7$ obtained by equating $\tau_c^{-1/2} \sim N^{-3/7}$. Based on this naive calculation, we depict $\Delta_N N^{3/7}$ as a function of $\tau N^{-6/7}$ in Fig. 8 up to $\tau < \tau_s$.

Unlike the other cases, Δ_N shows neither saturating nor exponentially decaying behavior. Rather, noisy behavior abruptly starts after exhibiting a power-law decay in time. If we interpreted the beginning of the noisy behavior as the development of fluctuations, this beginning time still seems to scale with the MFSCE dynamic exponent $\bar{z} = 6/7$. For comparison, we plot $\Delta_N N^{1/3}$ against $\tau N^{-2/3}$ in the inset of Fig. 8. Although the collapse in the inset looks poorer than the main figure, we, of course, cannot make a firm conclusion because of the lack of either saturating or exponentially decaying behavior.

In a sense, the ES case seems to mix some features of other two cases. First, similar to the case with $s > \frac{1}{2}$, $\bar{\nu}_c$ is close to 1.5 as found in Sec. IV. Second, similar to the case with $s < \frac{1}{2}$, Δ_N fluctuates around zero for any N .

VII. DISCUSSION

A. Sampling rule versus FSS

Since our rule of choosing natural frequencies involves overall shift of x_k ’s by the amount s in comparison to the ES case, it is natural to raise a question as to such a global shift of x_k ’s is necessary to observe a different FSS. Also one may ask any type of global shift always triggers a different FSS. In fact, the answers are no for both questions as explained below.

Let us answer the first question first. One answer is already found by comparing the rule with $s = 0$ and $s = 1$ for even N . By the rule, $N - 2$ oscillators have the same natural frequencies for these two cases. To be more precise, we have $\omega_k(s = 1) = \omega_{k-1}(s = 0)$ for $2 \leq k \leq M$. The only difference is that ω_M for $s = 0$ is replaced by $\omega_1 = 0$ for $s = 1$. That is, changing frequencies of two oscillators can trigger different FSS. Since the entrainment is driven by oscillators with small ω , the change of scaling behavior by assigning more oscillators around $\omega = 0$ may not be surprising. Still, we find it interesting for such a minute change to affect the global scaling behavior.

Presumably, this drastic change of scaling behavior by a minute modification should be attributed to the deterministic nature of dynamics as well as the fully connected interaction. It would be hardly conceivable to observe this effect if there is a ‘thermal’ noise or if the system is on a d -dimensional lattice.

We now give a more general answer, which is more insightful than the previous one. We find it most effective to explain it using mathematical formulae. Let

$$y_k := \frac{k - 1/2}{N},$$

for $k = 1, 2, \dots, N$ and let Ω_0 be the set of tuples (k, y_k, ω_k) with ω_k determined by the regular sampling rule Eq. (9). For convenience, the index set I now consists of all positive integers from 1 to N , which should

not be confused with Sec. II. Let

$$S(z, \Omega_0) = \frac{1}{N} \sum_{k \in I} \Theta(z^2 - \omega_k^2) \sqrt{1 - \frac{\omega_k^2}{z^2}},$$

which is just a repeat of Eq. (22). For clarity, we explicitly write that S is also a function of the set of tuples (k, y_k, ω_k) . Now we consider two different sets Ω_{\pm} of tuples $(k, y_k^{\pm}, \omega_k^{\pm})$ with

$$y_k^{\pm} = \int_0^{\omega_k^{\pm}} g(\omega) d\omega.$$

In Ω_+ , we assign $y_k^+ = y_k$ for $k > 1$ and choose y_1^+ such that $\omega_1^+ = a/N$ with a to be an arbitrary N -independent constant. In Ω_- , we assign $y_k^- = y_k$ for all $k \neq M$ ($M = \lfloor N/2 \rfloor$: the integer part of $N/2$) and choose y_M^- such that $\omega_M^- = b$ with b to be an arbitrary N -independent constant. For later reference, we write $k_+ = 1$ and $k_- = M$. Note that the full symmetry $\omega_k^{\pm} + \omega_{N-k+1}^{\pm} = 0$ is not satisfied in Ω_{\pm} , which actually does not play any role in the following discussion.

Assume N is sufficiently large, $|z| \ll 1$, and $Nz \gg 1$. Let $\Delta_{\pm} S := S(z, \Omega_{\pm}) - S(z, \Omega_0)$. Obviously,

$$\begin{aligned} \Delta_{\pm} S &= \frac{1}{N} \Theta\left(z - \left|\omega_{k_{\pm}}^{\pm}\right|\right) \sqrt{1 - \left(\frac{\omega_{k_{\pm}}^{\pm}}{z}\right)^2} \\ &\quad - \frac{1}{N} \Theta\left(z - \left|\omega_{k_{\pm}}^{\pm}\right|\right) \sqrt{1 - \left(\frac{\omega_{k_{\pm}}^{\pm}}{z}\right)^2} \approx \pm \frac{1}{N}, \end{aligned} \quad (35)$$

regardless of the actual value of a and b , where the error is $O(z^{-2}N^{-3})$. In other words, the MFSCE with Ω_+ (Ω_-) is identical to that of $s = 1$ ($s = 0$) at least up to the second order correction. Again, a single change of a frequency can trigger different FSS. We also performed simulations, to confirm the above conclusion at least for Ω_+ (details not shown here).

In a more general setting, the above answer can be used to yield another MFSCE with different FSS exponents. Assume $0 \leq \mu < 1$ and we construct Ω_{μ} such that $y_{\mu, k} = a_k/N$ for $1 \leq k \leq N^{\mu}$ with a_k 's to be arbitrary $O(1)$ numbers and $y_{\mu, k} = y_k$ for $k > N^{\mu}$. Needless to say, Ω_{μ} satisfies Eq. (2). Then, by the same logic in Eq. (35), we have

$$S(z, \Omega_{\mu}) \approx J(z) + N^{\mu-1},$$

which obviously predicts μ -dependent FSS exponents $\bar{\nu}_c = \bar{\nu}_+ = 1.5/(1 - \mu)$. Note that in $S(z, \Omega_{\mu}) - S(z, \Omega_0)$, $y_{\mu, k}$'s for $k \leq N^{\mu}$ contribute $1/N$ for each, thus $N^{\mu-1}$. Since more entrained oscillators are involved in the MFSCE as μ gets larger, which entails that the MFSCE becomes more and more reliable, and the MFSCE for the case of $\mu = 0$ (or the case with $s = 1$) already predicts the right $\bar{\nu}_+ = \bar{\nu}_c$, we believe the MFSCE for Ω_{μ} predicts correct $\bar{\nu}_+ = \bar{\nu}_c$. By preliminary numerical studies, we confirmed the above prediction for $\bar{\nu}_c$ with $\mu = 1/4$ (not shown here).

If $\mu > \frac{1}{2}$, the MFSCE would predict the right $\bar{\nu}_-$ that is same as $\bar{\nu}_+$, because the solution ($\propto (K_c - K)^{-1}N^{\mu-1}$) of the MFSCE in the subcritical region is already larger than $N^{-1/2}$. But numerical confirmation of this prediction for $\mu > \frac{1}{2}$ would be very demanding, since N should be so large that Eq (2) is well satisfied.

Now we move on to the second question. To this end, let us consider another rule of regular sampling such that

$$\int_{-\infty}^{\omega_k} g(\omega) d\omega = \frac{k}{N}, \quad (36)$$

which also globally shifts by $1/2$ from the ES case. By noticing that the above rule can be implemented from the $s = 0$ case by reassigning ω_M to be 0 with ω_{-M} intact, one can easily conclude that the MFSCE with the rule (36) becomes identical to $S(z, \Omega_0)$ up to the leading correction of $O(1/\sqrt{zN^3})$. In this sense, the above global shift does not affect the FSS in comparison to the ES case within the current context. We also checked numerically that this conclusion is valid (details not shown here).

B. $\bar{\nu}_+$ versus $\bar{\nu}_c$ for $s = 0$

For $s = 1$, we have argued (hopefully convincingly) that $\bar{\nu}_+ = \bar{\nu}_c$. On the other hand, numerical simulations for $s = 0$ at criticality showed that $\bar{\nu}_+ \neq \bar{\nu}_c$. According to the conventional scaling theory with $\rho_+(x)$, one would expect for sufficiently small value of the scaling parameter x

$$\rho_+(x) \sim x^{-\beta/\bar{\nu}_+}, \quad (37)$$

which predicts $\bar{\nu}_+ = \bar{\nu}_c$. Since $\rho_+(x)$ seems well defined even for $s = 0$, one may ask how the scaling relation cannot be valid.

Actually, the answer is already given in Fig. 4(b). When $K - K_c$ is very small, N should be sufficiently large for ρ_+ of the MFSCE to predict Δ_N correctly even qualitatively. Therefore, no matter how large N is, $x \rightarrow 0$ limit fails to have the asymptotic behavior in Eq. (37) and therefore $\bar{\nu}_+$ has no reason to be associated with $\bar{\nu}_c$. This should be compared with the case of $s = 1$, where the MFSCE gives correct behavior for any N at least qualitatively.

Similar discussion can be applied to the dynamic fluctuation, which suggests that the fluctuation exponent γ in the supercritical region may not dictate the large- N behavior of fluctuations at criticality. This is surely an intriguing question and a detailed discussion for γ will be reported elsewhere.

VIII. SUMMARY AND CONCLUSION

Up to now, we have analyzed the finite-size-scaling exponents $\bar{\nu}_{\pm}$ and $\bar{\nu}_c$ of the order parameter R_N for the

‘deterministic’ sampling of natural frequencies with characterizing parameter s , using both the mean-field self-consistent equation and numerical simulations. The results are summarized in Table I.

Most significant contribution of this work would be that by extensive simulations with large size and long time we corrected the reported value in the literature of $\bar{\nu}$ of the regular-sampling case (the case with $s = \frac{1}{2}$ in the Table I). We have also shown that $\bar{\nu}_+$ needs not be the same as $\bar{\nu}_c$ especially for the case with $s < \frac{1}{2}$. We also argued that $\bar{\nu}_+$ in the supercritical region needs not be identical to $\bar{\nu}_-$ in the subcritical region. On this account, we claim that the finite-size scaling of the Kuramoto model should be reconsidered more carefully, especially for the ‘deterministic’ sampling of natural frequencies.

ACKNOWLEDGMENTS

S-CP acknowledges support by the National Research Foundation of Korea (NRF) grant funded by the Korea government (MSIT) Grant No. RS-2023-00249949. S-CP also thanks for the hospitality of Korea Institute for Advanced Study (KIAS) during his sabbatical leave in 2023. HP acknowledges support by NRF Grant No. 2017R1D1A1B06035497 and individual KIAS Grant No. QP013601 at the KIAS. The authors are grateful to the Center for Advanced Computation at KIAS for help with computing resources.

Appendix A: Derivation of finite-size corrections in the MFSCe

In this Appendix, we derive Eq. (27) regardless of whether N is even or odd. To treat both even- and odd- N cases on a same footing, we introduce σ which takes 1 (0) if N is odd (even) and write $x_k = (k - s + \frac{1}{2}\sigma)/N$.

We first define for $0 \leq x \leq G(z)$

$$f(x) := \sqrt{1 - \frac{G^{-1}(x)^2}{z^2}}.$$

TABLE I. The FSS exponents $\bar{\nu}_+$, $\bar{\nu}_-$, and, $\bar{\nu}_c$ estimated by the MFSCe and by simulations for different s . X means the failure of the mean field theory and – means not discussed in this paper. The estimates of $\bar{\nu}_-$ ’s from simulations are not available in this work, so we omit them in this table. For comparison, the last column also presents the result of $\bar{\nu}$ in the literature for the ES case.

s	MFSCe			simulations		
	$\bar{\nu}_+$	$\bar{\nu}_-$	$\bar{\nu}_c$	$\bar{\nu}_+$	$\bar{\nu}_c$	$\bar{\nu}$
$= \frac{1}{2}$	X	X	$\leq \frac{7}{6}$	–	≈ 1.52	1.25 ^a
$> \frac{1}{2}$	$\frac{3}{2}$	$\frac{3}{2}$	$\frac{3}{2}$	$\frac{3}{2}$	$\frac{3}{2}$	
$< \frac{1}{2}$	$\frac{3}{2}$	X	X	$\frac{3}{2}$	≈ 1.02	

^a From Ref [5]

For brevity, z is omitted in the argument of f . Notice that by the change of variables $x = G(\omega)$, we have

$$J(z) = 2 \int_0^{G(z)} f(x) dx.$$

In the following, we assume $z \ll 1$ and $Nz \gg 1$. For later reference, we summarize the derivatives of f for small z as follows:

$$\begin{aligned} f(x) &\approx \frac{\sqrt{G(z)^2 - x^2}}{G(z)}, \\ f'(x) &\approx -\frac{x}{G(z)\sqrt{G(z)^2 - x^2}}, \\ f''(x) &\approx -\frac{G(z)}{[G(z)^2 - x^2]^{3/2}}, \end{aligned} \quad (\text{A1})$$

where we have used $G^{-1}(x) \approx x/g_0$ and $G(z) \approx g_0z$ with $g_0 := g(0)$. Obviously, $f''(x)$ is a decreasing function of x at least for sufficiently small z .

It is convenient to define

$$k_m := \max\{k : \omega_k \leq z\}, \quad \alpha := NG(z) + s - \frac{1}{2}\sigma - k_m.$$

Note that α is a function of z with the range $0 \leq \alpha \leq 1$. Let

$$\begin{aligned} a_k^\pm &:= x_k \pm \frac{1}{2N}, \quad z_0 := G^{-1}(a_{k_m}^-), \\ J_0 &:= 2 \int_0^{a_1^+} f(x) dx, \quad J_1 := 2 \int_{G(z_0)}^{G(z)} f(x) dx, \\ J_2 &:= 2 \int_{a_2^-}^{G(z_0)} f(x) dx = 2 \sum_{k=2}^{k_m-1} \int_{a_k^-}^{a_k^+} f(x) dx. \end{aligned} \quad (\text{A2})$$

Since $a_{k+1}^- = a_k^+$, we have $J(z) = J_0 + J_1 + J_2$.

We first find an approximation for J_0 . Since $f(x) = 1 + O(x^2/z^2)$ for $x \ll z$, we have

$$J_0 = 2a_1^+ + O\left(\frac{1}{z^2N^3}\right) = \frac{3 - 2s + \sigma}{N} + O\left(\frac{1}{z^2N^3}\right).$$

Since

$$\frac{1}{N} \sum_{k=-1}^1 \sqrt{1 - \frac{\omega_k^2}{z^2}} = \frac{2 + \sigma}{N} + O\left(\frac{1}{z^2N^3}\right),$$

we can write

$$J_0 = \frac{1}{N} \sum_{k=-1}^1 \sqrt{1 - \frac{\omega_k^2}{z^2}} + \frac{1 - 2s}{N} + O\left(\frac{1}{z^2N^3}\right). \quad (\text{A3})$$

Note that (A3) is valid for a general g we are interested in.

If we write $g(\omega) = g_0(1 - 4C\omega^2)$, we have

$$\begin{aligned} J_1 &= z g_0 (1 - Cz^2) \cos^{-1}\left(\frac{z_0}{z}\right) \\ &\quad + g_0 z_0 \sqrt{1 - \frac{z_0^2}{z^2}} (2Cz_0^2 - Cz^2 - 1). \end{aligned}$$

Note that the above formula becomes an approximation for a general g . Let $\epsilon := 1 - z_0/z$ or $z_0 = z(1 - \epsilon)$. Assuming $\epsilon \ll z \ll 1$, we can approximate $J_1 \approx g_0 4\sqrt{2}z\epsilon^{3/2}/3$. Since $G(z) - G(z_0) = (1 + 2\alpha)/(2N)$ and $G(\omega) \approx g_0\omega$ for small ω , we further approximate

$$\epsilon = 1 - \frac{z_0}{z} \approx \frac{G(z) - G(z_0)}{G(z)} \approx \frac{1 + 2\alpha}{2g_0zN}, \quad (\text{A4})$$

which gives

$$J_1 = \frac{2(1 + 2\alpha)^{3/2}}{3} (g_0zN^3)^{-1/2} + o\left(\frac{1}{\sqrt{zN^3}}\right). \quad (\text{A5})$$

Note that the coefficient C does not contribute to the leading order of (A5).

To analyze J_2 , we use the Taylor's theorem. For any x with $a_k^- \leq x \leq a_k^+$, there is y_k such that $a_k^- \leq y_k \leq a_k^+$ and

$$f(x) = f(x_k) + f'(x_k)(x - x_k) + \frac{f''(y_k)}{2}(x - x_k)^2, \quad (\text{A6})$$

where y_k should be understood as a function of x . Plugging (A6) into (A2), we have

$$J_2 = \frac{2}{N} \sum_{k=2}^{k_m-1} f(x_k) + E_1, \quad (\text{A7})$$

$$E_1 := \sum_{k=2}^{k_m-1} \int_{a_k^-}^{a_k^+} f''(y_k)(x - x_k)^2 dx.$$

Since $a_k^- \leq y_k \leq a_k^+$ and $f''(x)$ is a decreasing function, we have $f''(a_k^+) \leq f''(y_k) \leq f''(a_k^-)$ and, in turn,

$$\frac{f''(a_k^+)}{12N^3} \leq \int_{a_k^-}^{a_k^+} f''(y_k)(x - x_k)^2 dx \leq \frac{f''(a_k^-)}{12N^3},$$

where we have used

$$\int_{a_k^-}^{a_k^+} (x - x_k)^2 dx = \frac{1}{12N^3}.$$

Therefore,

$$E_2 - \frac{f''(a_2^-)}{12N^3} \leq E_1 \leq E_2 - \frac{f''(G(z_0))}{12N^3},$$

$$E_2 := \frac{1}{12N^3} \sum_{k=2}^{k_m} f''(a_k^-).$$

Since $f''(x)$ is monotonously decreasing and

$$h(b) + \int_a^b h(k) dk \leq \sum_{k=a}^b h(k) \leq h(a) + \int_a^b h(k) dk$$

for any monotonously decreasing function h ($a \leq b$ are integers), we have

$$\frac{f''(G(z_0))}{12N^3} \leq E_2 - \frac{f'(G(z_0)) - f'(a_2^-)}{12N^2} \leq \frac{f''(G(a_2^-))}{12N^3}.$$

Using (A1), we have

$$\frac{f''(G(z_0))}{12N^3} = -\frac{(1 + 2\alpha)^{-3/2}}{12} \frac{1}{\sqrt{g_0zN^3}} + o\left(\frac{1}{\sqrt{zN^3}}\right),$$

$$\frac{f'(G(z_0))}{12N^2} = -\frac{(1 + 2\alpha)^{-1/2}}{12} \frac{1}{\sqrt{g_0zN^3}} + o\left(\frac{1}{\sqrt{zN^3}}\right).$$

Since the terms with a_2^- are negligible, we have

$$E_1 = -\left[\frac{(1 + 2\alpha)^{-1/2}}{12} + \eta_1(\alpha)\right] \frac{1}{\sqrt{g_0zN^3}} + o\left(\frac{1}{\sqrt{zN^3}}\right),$$

$$|\eta_1(\alpha)| \leq \tilde{\eta}(\alpha), \quad \tilde{\eta}(\alpha) := \frac{1}{12}(1 + 2\alpha)^{-3/2}. \quad (\text{A8})$$

Since $f^{(n)}(G(z_0))/N^{n+1} = O(1/\sqrt{zN^3})$ for any n , it is difficult, if not impossible, to find an explicit formula for η_1 , even considering more terms in the Taylor expansion. Since

$$\frac{2}{N} f(x_{k_m}) = \sqrt{8\alpha}(g_0zN^3)^{-1/2} + o\left(\frac{1}{\sqrt{zN^3}}\right),$$

(A3), (A5), and (A7) combined with (A8) give Eq. (27). Now we have the approximate MFSCE for general g as

$$\frac{Z}{K} \approx \frac{Z}{K_c}(1 - CZ^2) + \frac{2s - 1}{N} + \frac{\eta_0(\alpha)}{\sqrt{g_0ZN^3}}, \quad (\text{A9})$$

which is Eq. (28) for $C = 1$ and $g_0 = g(0)$. Notice that η_0 is “universal” in that the above approximation is applicable to a general g with the corresponding g_0 and C . By the same token, the conclusion based on the MFSCE in the main text is not limited to the frequency density (10).

[1] Y. Kuramoto, *Chemical Oscillations, Waves, and Turbulence* (Springer Verlag, Berlin, 1984).

[2] S. H. Strogatz, From Kuramoto to Crawford: exploring

- the onset of synchronization in populations of coupled oscillators, *Physica D* **143**, 1 (2000).
- [3] D. Pazó, Thermodynamic limit of the first-order phase transition in the Kuramoto model, *Phys. Rev. E* **72**, 046211 (2005).
- [4] B. Ottino-Löffler and S. H. Strogatz, Kuramoto model with uniformly spaced frequencies: Finite- N asymptotics of the locking threshold, *Phys. Rev. E* **93**, 062220 (2016).
- [5] H. Hong, H. Chaté, L.-H. Tang, and H. Park, Finite-size scaling, dynamic fluctuations, and hyperscaling relation in the Kuramoto model, *Phys. Rev. E* **92**, 022122 (2015).
- [6] H. Daido, Discrete-time population dynamics of interacting self-oscillators, *Prog. Theor. Phys.* **75**, 1460 (1986).
- [7] E. J. Hildebrand, M. A. Buice, and C. C. Chow, Kinetic Theory of Coupled Oscillators, *Phys. Rev. Lett.* **98**, 054101 (2007).
- [8] M. A. Buice and C. C. Chow, Correlations, fluctuations, and stability of a finite-size network of coupled oscillators, *Phys. Rev. E* **76**, 031118 (2007).
- [9] H. Hong, H. Chaté, H. Park, and L.-H. Tang, Entrainment Transition in Populations of Random Frequency Oscillators, *Phys. Rev. Lett.* **99**, 184101 (2007).
- [10] H. Hong, H. Park, and M. Y. Choi, Collective synchronization in spatially extended systems of coupled oscillators with random frequencies, *Phys. Rev. E* **72**, 036217 (2005).
- [11] S.-C. Park, High-precision estimate of the critical exponents for the directed ising universality class, *J. Korean Phys. Soc.* **62**, 469 (2013).
- [12] S.-C. Park, Critical decay exponent of the pair contact process with diffusion, *Phys. Rev. E* **90**, 052115 (2014).
- [13] H. Daido, Intrinsic fluctuations and a phase transition in a class of large populations of interacting oscillators, *J. Stat. Phys.* **60**, 763 (1990).
- [14] P. C. Hohenberg and B. I. Halperin, Theory of dynamic critical phenomena, *Rev. Mod. Phys.* **49**, 435 (1977).